Journal of Applied Physics

RESEARCH ARTICLE | AUGUST 15 2023

RF-sputtered Z-cut electro-optic barium titanate modulator on silicon photonic platform FREE

Agham B. Posadas ; Vincent E. Stenger ; John D. DeFouw ; Jamie H. Warner ; Alexander A. Demkov

Journal of Applied Physics 134, 073101 (2023)
https://doi.org/10.1063/5.0160186

Journal of Applied Physics ARTICLE pubs.aip.org/aip/jap

RF-sputtered Z-cut electro-optic barium titanate modulator on silicon photonic platform

Cite as: J. Appl. Phys. **134**, 073101 (2023); doi: 10.1063/5.0160186
Submitted: 30 May 2023 · Accepted: 26 July 2023 ·
Published Online: 15 August 2023

Agham B. Posadas,[1,2] Vincent E. Stenger,[3] John D. DeFouw,[3] Jamie H. Warner,[4] and Alexander A. Demkov[1,2,a)]

AFFILIATIONS

[1]Department of Physics, The University of Texas at Austin, Austin, Texas 78712, USA
[2]La Luce Cristallina, Inc., Austin, Texas 78759, USA
[3]SRICO, Inc., Columbus, Ohio 43235, USA
[4]Walker Department of Mechanical Engineering, The University of Texas at Austin, Austin, Texas 78712, USA

[a)]**Author to whom correspondence should be addressed:** demkov@physics.utexas.edu

ABSTRACT

Epitaxial $BaTiO_3$ integrated on Si or Si-on-insulator using off-axis radio frequency sputtering is a promising material platform for building electro-optic modulators based on the Pockels effect. Barium titanate thin films with c-axis orientation have been epitaxially integrated on silicon-on-insulator wafers. They exhibit excellent structural quality with Pockels coefficient (r_{33}) > 130 pm/V and propagation loss <2 dB/cm. Our results show that off-axis sputtered $BaTiO_3$ films yield electro-optic modulation similar to that of high-quality films grown by molecular beam epitaxy and that the material is suitable for implementation of low-power Mach–Zehnder interferometer electro-optic modulators integrated on silicon in a Z-cut configuration.

I. INTRODUCTION

The current revolution in integrated Si photonics—the information processing technology based on IR light guided through structures fabricated in Si—calls for energy-efficient, fast, and compact electro-optic (EO) modulators.[1] Though most current applications of Si photonics are targeting the O band (wavelengths ranging from 1260 to 1360 nm), the C-band (1530–1565 nm) still offers the lowest fiber loss (0.1419 dB/km at 1560 nm) and a low-power, small footprint modulator at 1550 nm could serve as a bridge between the optical fiber and the circuit board, as well as enable on-chip optical communications.[2,3] Si-integrated phase shifters based on ferroelectrics that take advantage of the linear EO effect offer a promising avenue to building this technology.[4,5]

Lithium niobate ($LiNbO_3$) or LN has been successfully demonstrated to perform well in this regard and can be used in integrated Si photonic devices. Thin-film integration of LN on silicon, however, requires energy-intensive and complex wafer bonding processes. The integration process is similar to silicon-on-insulator or SOI technology. A Czochralski-grown LN wafer is flip-wafer-bonded to an SiO_2-covered Si carrier wafer,[6] then using the smart-cut technology[7] and chemical mechanical polishing, only a relatively thin LN film is left on this carrier Si wafer. There is currently a wafer size limit of 6-in. due to the limited size at which LN single crystals can be grown.

LN is transparent in a very wide spectral range from 0.35 to 5 μm and shows strong linear EO or Pockels effect and allows pure phase modulation with no variation in absorption.[8] While bulk LN EO devices have been used in the fiber optics industry for a long time, commercial thin-film LN wafers have become available only recently. However, the overall performance of thin-film LN modulators is already comparable with the performance of the traditional photonic platforms such as silicon and indium phosphide.[9–11] The best reported device performance metrics for a hybrid waveguide modulator (taken from different devices) have demonstrated $V_\pi L$ of 3 V cm, loss as low as 0.2 dB/cm and bandwidth of 106 GHz, while the monolithic devices boast $V_\pi L$ of 1.2 V cm, loss of 0.15 dB/cm and bandwidth of 100 GHz.[4] A hybrid device is one where the waveguides and modulators are patterned on top of the LN layer with a different material (usually Si or SiN_x), while a monolithic device is one where the waveguide and modulator are patterned in the LN material itself.

Barium titanate ($BaTiO_3$) or BTO, on the other hand, is a ferroelectric material that exhibits one of the largest Pockels coefficients among EO materials, with a coefficient as high as 1300 pm/V in the bulk.[12] In addition to the substantially larger Pockels coefficient compared to LN, BTO is much easier to integrate with Si.[13–18] Epitaxially grown BTO integrated on Si or SOI is a promising materials platform for building EO modulators based on the Pockels effect that can be used for fast, low-power optical switches, with applications ranging from sensors to novel forms of computing including neuromorphic and quantum computing.[19,20]

To date, published work on BTO EO devices has focused on the hybrid approach pioneered by Abel *et al.*,[13] where a transverse electric (TE) polarized optical mode signal is guided through a Si or SiN_x waveguide etched in a layer deposited on top of the BTO, which is epitaxially grown on Si by MBE or RF sputtering. This architecture corresponds to so-called X- or Y-cut devices in LN-based technology [Fig. 1(a)]. These devices demonstrate that substantial EO modulation can be achieved in a Si photonics-compatible process that utilize a portion of the r_{42} component of the BTO Pockels tensor, which is the largest component, and relies on the BTO film having its ferroelectric polarization in-plane.

A tantalizing possibility exists in fabricating what is known as a Z-cut waveguide phase-shifter, with the ridge waveguide being etched directly in BTO and designed to support a transverse magnetic (TM) polarized optical mode signal [see Fig. 1(b)]. One issue with TE mode devices is that fields applied along the X-direction of the crystal to access r_{42} experience an extremely high dielectric constant, typically over 1000. This high dielectric constant directly translates to decreased EO modulation efficiency at RF frequencies. In contrast, fields applied along the Z-direction to access the r_{33} Pockels component experience a more typical dielectric constant less than 60. This reduction in dielectric loading can more than offset the reduction in the EO coefficient. Another benefit to Z-cut films is that they are more readily poled along the surface normal direction to produce a uniform polarization across the wafer. These two features provide the motivation for Z-cut EO modulator devices based on r_{33}. Moor *et al.* recently reported an electro-optic modulator based on BTO on SOI that utilizes the r_{33} coefficient in combination with plasmonic structures and showed very low potential $V_\pi L$ for such devices.[21]

In this paper, we describe the growth of c-oriented (Z-cut) BTO films by off-axis RF magnetron sputtering on silicon-on-insulator (SOI) wafers. A Z-cut EO modulator test device, based on a ridge-loaded waveguide design, is fabricated and the r_{33} EO coefficient for the BTO film is extracted.

II. GROWTH OF BTO FILMS

Standard photonic-grade SOI wafers from Soitec (220-nm device Si layer with a 3-μm buried oxide layer) were used as the substrate for growing the BTO thin films. The wafers were cored into 2-in.-diameter wafers that were then degreased by soaking in acetone, isopropanol, and de-ionized water for 5 min each with sonication. The wafers were then dried and exposed to UV/ozone for 15 min to decompose organic contaminants. The films were grown in a custom hybrid deposition system manufactured by DCA Instruments that combines both oxide molecular beam epitaxy (MBE) and RF sputtering in the same chamber. After loading into the deposition chamber, the wafers were first outgassed at 700 °C in ultrahigh vacuum, then the native oxide was desorbed using Sr-assisted deoxidation.[22] One-half monolayer of Sr metal was then deposited at 600 °C to form a protective layer on Si prior to the next step, which is the deposition of the $SrTiO_3$ (STO) buffer.

An 8-nm-thick STO buffer layer was grown in two steps using MBE with Sr and Ti metal evaporated from effusion cells. A 2-nm seed layer was first grown at 200 °C under continuous oxygen partial pressure ramping (7×10^{-8}–5×10^{-7} Torr), which is then crystallized after a 5-min vacuum anneal at 550 °C. An additional 6 nm of STO was then deposited at 550 °C under 5×10^{-7} Torr oxygen.

After STO buffer formation, BTO was deposited using the RF sputtering system to a thickness of 110 nm from a 2 in.-diameter stoichiometric ceramic target (Plasmaterials). Prior to each growth, the target is presputtered for 10 min to ensure the target surface is clean and surface composition is constant. The sputtering was performed at a power density of 2.2 W/cm^2 in a 3:7 O_2:Ar mixture at a total pressure of 1×10^{-2} Torr, with typical flow rates of 21.4 and

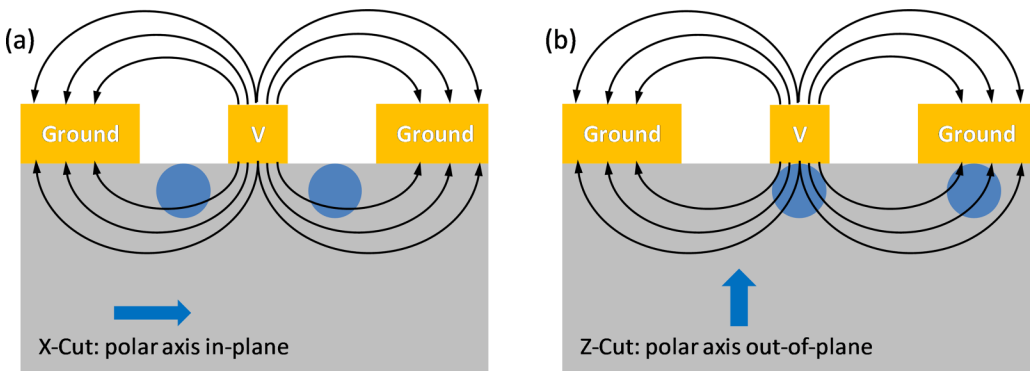

FIG. 1. Schematic diagram of (a) X-cut vs (b) Z-cut modulator. The placement of the waveguide regions are shown as blue circles for each configuration.

9.2 SCCM for Ar and O_2, respectively. The system has an off-axis geometry where the substrate axis is at 90° relative to the sputtering gun axis. The substrate plane was about 5 cm above the sputtering gun axis and the substrate center was about 3.5 cm from the target surface. Deposition was done at a substrate temperature of 680 °C (calibrated using a pyrometer) and the sample was cooled down at 5 °C/min in the process gas until room temperature. Typical BTO growth rates were ∼2 nm/min. The film thickness was kept at 110 nm in order to obtain fully c axis oriented films.

III. FILM STRUCTURAL CHARACTERIZATION

The BTO samples were measured after growth using *in situ* reflection high energy electron diffraction (RHEED) and *in situ* x-ray photoelectron spectroscopy (XPS) prior to being unloaded from the vacuum system. RHEED images were taken using an electron energy of 20 keV and a grazing angle of 4°, with a typical pattern taken along the BTO ⟨110⟩ azimuth shown in Fig. 2(a). This shows a very flat and highly ordered crystalline surface as grown. XPS shows a typical surface composition of 1.02 Ba to 0.98 Ti. After unloading from the vacuum system, samples were analyzed using x-ray diffraction to determine both in-plane and out-of-plane lattice constants, as well as using x-ray reflectivity to determine the actual film thickness. The measurements were performed using a Rigaku Ultima IV diffractometer with in-plane arm using Cu Kα radiation. A typical x-ray reflectivity scan is shown in Fig. 2(b), showing a measurement and simulation. For this set of data, the parameter values needed to match the simulation results

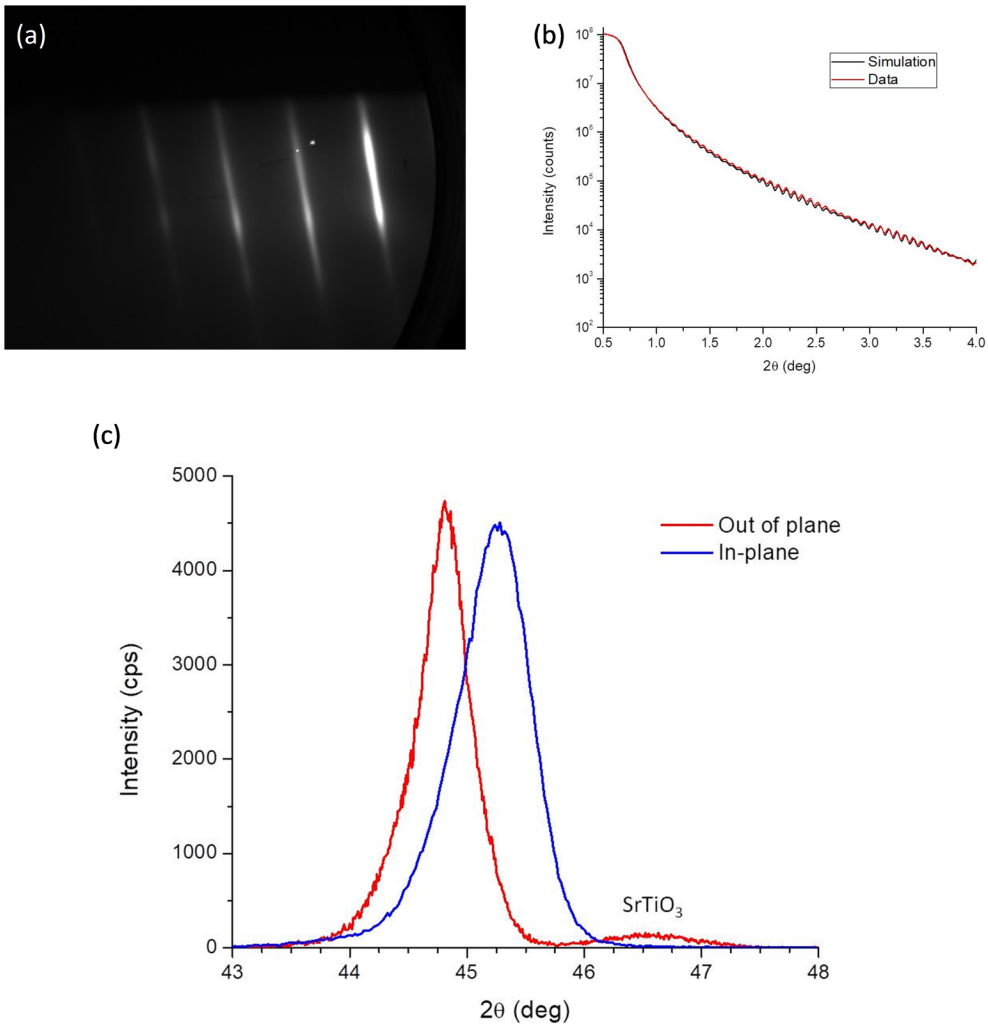

FIG. 2. (a) RHEED pattern of RF-sputtered 110-nm BTO on Si taken along the ⟨110⟩ azimuth of BTO; (b) x-ray reflectivity from a nominally 110 nm-thick BTO film with 8 nm $SrTiO_3$ buffer on Si. The parameters needed to match the data are listed in the text; (c) in-plane and out-of-plane x-ray diffraction scans of BTO film on Si.

to the data were 106.9 nm BTO thickness with 8.1 nm STO buffer and a surface roughness of 0.4 nm.

Figure 2(c) shows scans along the out-of-plane and the in-plane 002/200 directions. The scans show an out-of-plane lattice constant of 4.035 Å and a single in-plane lattice constant of 4.004 Å, indicating a c axis oriented film with c/a ratio of 1.007 742. This is slightly lower than the bulk value of 1.010 indicating some residual tensile strain in the film. Rocking curve scans around the 002 Bragg peak show typical full-width at half-maximum values of 0.6°.

Cross-sectional transmission electron microscopy imaging was also performed on one of the patterned samples to check the epitaxy and crystalline quality of the BTO layer. The cross-sectional samples for scanning transmission electron microscopy (STEM) were prepared using a Scios 2 HiVac focused ion beam system from Fisher Scientific. Annular dark-field STEM (ADF-STEM) was performed using a JEOL NEOARM equipped with a probe corrector for STEM, operated at an accelerating voltage of 200 kV. Figure 3 shows a cross-sectional transmission electron microscopy (TEM) scan of a heterostructure used to make the Z-cut EO devices. Figure 3(a) is a lower magnification image showing the layers comprising the heterostructure. Figure 3(b) is a high magnification image showing the epitaxial nature of the BTO active layer.

IV. FILM OPTICAL CHARACTERIZATION

The complex refractive index for sputter-grown c-oriented epitaxial BTO films grown on SOI was characterized over visible and near-infrared wavelengths via variable angle spectroscopic ellipsometry. The resulting index value was 2.280 at a wavelength of 1550 nm. This result was in line with values reported for optical grade BTO films. In the ellipsometry data, the k value was limited by the resolution of the test to be <0.001. This precision was insufficient to qualify the material for integrated optics, which typically requires loss on the order of 1 dB/cm or less. Instead, a slab waveguide loss test was done using a Metricon 2010 prism coupler measurement system with optical loss attachment [Fig. 4(a)]. Slab loss was measured to be about 1.08 dB/cm for the TM mode and 1.65 dB/cm for the TE mode at 1550 nm wavelength. This result confirmed the material to be suitable for implementation of Mach–Zehnder interferometer (MZI) EO modulators.

The Metricon system was also used to test EO modulation of the BTO film [Fig. 4(b)]. For this test, the system was set up so that incident light partially coupled into the fundamental slab mode. At this setting, any change in the material index caused a shift in the slab mode index. Modeling and simulation were used to extract the material index change from the slab mode index change. Modulation of the BTO index was achieved by applying a voltage across the wafer sample. The modulation tests were done at audio frequencies due to limitations of the amplifier electronics.

The electric field applied across the BTO thickness was modeled by assuming a simple 1D layer stack-up of the layers shown in Fig. 4. Here, the Si layers were treated as partially conductive dielectrics while the BTO and SiO_2 layers were insulating dielectrics. For the modeling and extraction of the EO coefficient, BTO was assumed to have a relative dielectric constant $\varepsilon_r = 56$ in the surface normal (c or "Z") direction.[23] Si was assumed to have $\varepsilon_r = 12$ and resistivity $\rho = 10\,\Omega\,\text{cm}$. SiO_2 was assumed to have $\varepsilon_r = 4$. The thin 8 nm STO growth template layer between the BTO and Si was assumed to have the same dielectric properties as the BTO layer and was included as part of an overall BTO layer thickness $t_{BTO} = 110$ nm.

Since the Si layers were semiconducting, and the frequency was in the tens of Hz, the Si layers could be excluded from the field calculation. This simplified the model to a dielectric capacitive divider across the SiO_2 and BTO layers. This model was further

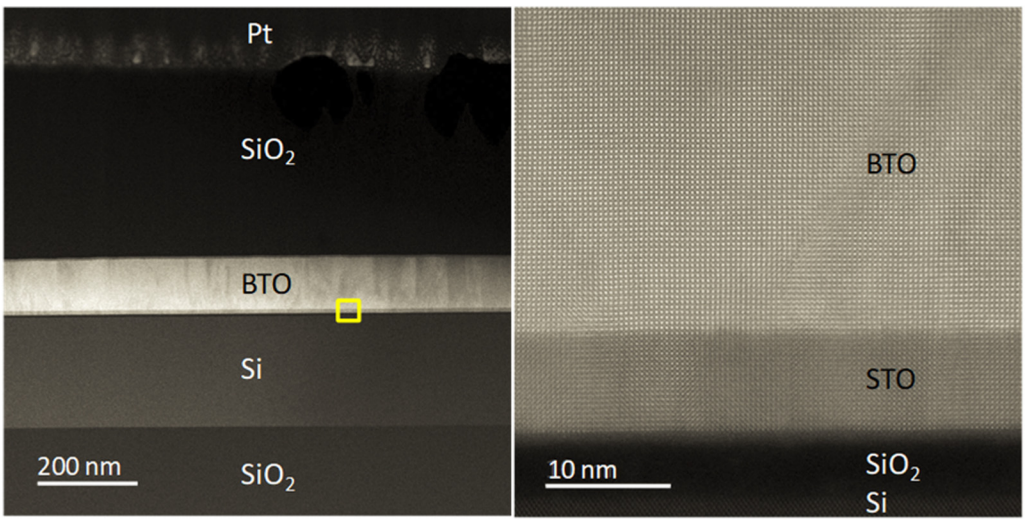

FIG. 3. Cross-sectional STEM image of the BTO film with amorphous SiO_2 deposited on top. (a) Image of the stack at a low magnification. (b) High magnification image of the yellow highlighted area.

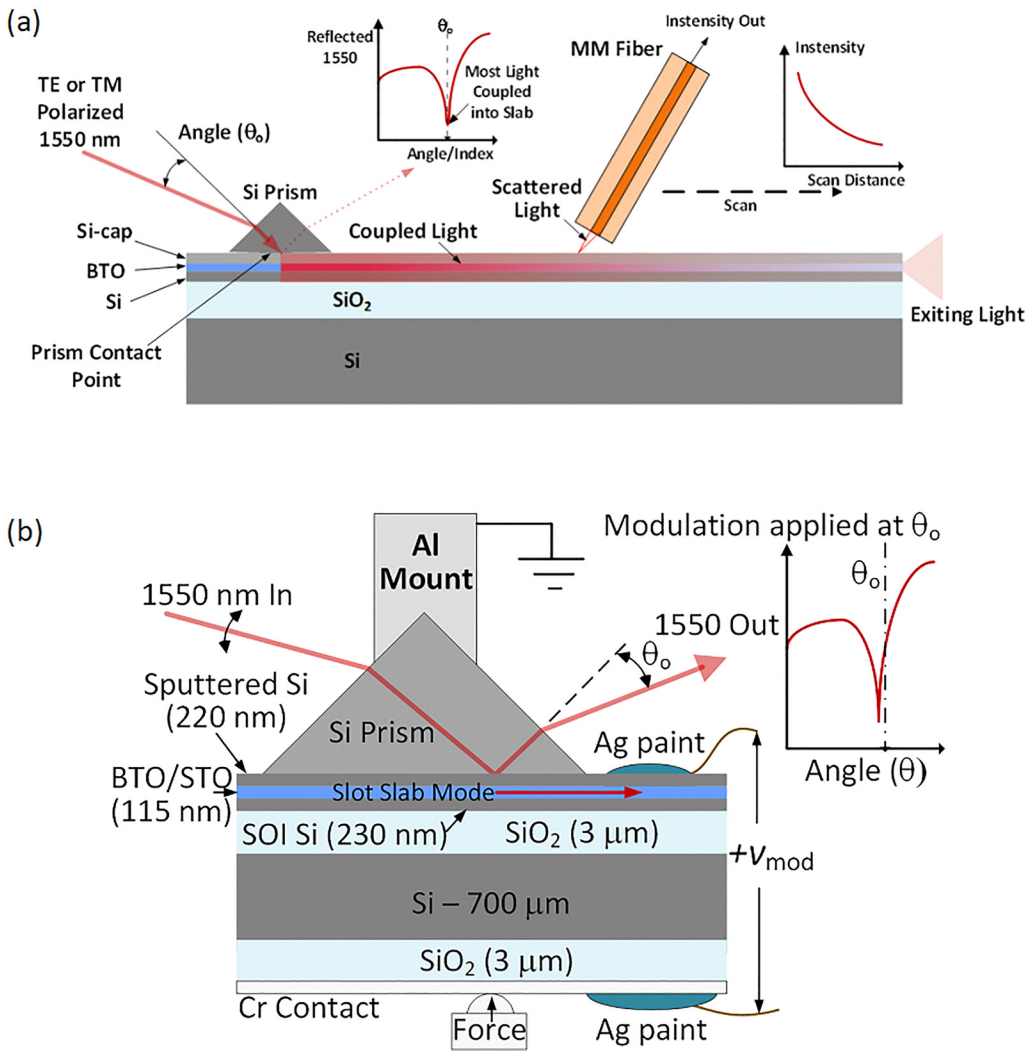

FIG. 4. (a) Slab loss measurement setup. Slab loss was measured to be about 1.08 dB/cm for the TM mode and 1.65 dB/cm for the TE mode at 1550 nm wavelength; (b) electro-optic r_{33} measurement setup using Metricon. Test results indicated an r_{33} value between 100 and 120 pm/V.

simplified by assuming that the bulk of the voltage drop was across SiO_2, due to $t_{BTO} \ll t_{SiO_2}$ and $\varepsilon_{BTO} \gg \varepsilon_{SiO_2}$. In this case, the field in the BTO for an applied voltage was reduced to

$$E_{BTO} \sim (V_{applied}/t_{SiO_2})(\varepsilon_{SiO_2}/\varepsilon_{BTO}), \quad (1)$$

where t_{SiO_2} is the total thickness of the SiO_2 layers.

The slab mode index will consist of some combination of all the material layers in the stack. As such, there will be a nonunity scale factor between the change in the slab mode index and the change in the BTO material index. This scale factor represents the sensitivity $\delta = \Delta n_{slab}/\Delta n_{BTO}$ of the slab optical mode to BTO material refractive index and can be rewritten as

$$\Delta n_{BTO} = \Delta n_{slab}/\delta. \quad (2)$$

For the stack-up shown in Fig. 4, the small signal change in slab mode index with change in BTO material index was determined from slab mode models to be 0.458.

By measuring Δn_{slab} for an applied voltage, Eqs. (1) and (2) were used to determine the r_{33} coefficient of the BTO film material through the following Pockels model:

$$r_{33} = 2\Delta n_{BTO}/(E_{BTO}\, n_{BTO}^3), \quad (3)$$

where n_{BTO} was taken as 2.25 for c-polarized light.

V. DEVICE FABRICATION AND TESTING

An MZI EO modulator test device was fabricated to facilitate measurement of the r_{33} coefficient of the sputtered Z-cut BTO material in a ridge waveguide device geometry. The test device geometry was based on a BTO ridge-loaded Si waveguide as shown in Fig. 5(a). This geometry represented a structure that would be relatively simple to fabricate as it did not require additional Si and BTO layers to be deposited. The device fabrication process steps entailed patterning and wet etching the BTO ridge down to 30 nm using a mixture of HF and HNO_3, followed by a blanket SiO_2 deposition by plasma enhanced chemical vapor deposition (PECVD) to a thickness of 350 nm, and metallization using Cr/Au via a patterning and metal lift-off process. Optical microscope images of a completed MZI test device are shown in Fig. 5(b).

The BTO ridge-loaded waveguide test device had significantly reduced EO overlap, relative to the more optimal slot waveguide design, due to the low relative permittivity SiO_2 buffer layer and to the reduced optical mode overlap with BTO. Specifically, the net EO overlap was reduced by over an order of magnitude, increasing simulated $V_\pi L$ to about 5 V cm for a device operating in the push–pull MZI mode. However, elimination of the Si and additional cap layers made extraction of r_{33} more accurate relative to the slot configuration since these cap layers represented unknown material properties.

EO measurements were taken by modulating one waveguide while holding the other at ground. Modulation testing was done at up to 10 MHz. Responses were observed to be relatively flat over RF frequency, with no fine spectral features being observed. Equal amplitude and opposite phase were observed in the MZI output response when switching the modulation voltage from one waveguide electrode to the other. This indicated that the BTO layers in each of the two MZI waveguides had equal EO coefficients. This further indicated the BTO layers were equally and uniformly poled along the same crystal direction.

To extract V_π, a 3Vpp triangle wave at 1.25 kHz was injected into one of the waveguide electrodes of a 1 mm length MZM device. The output modulated optical power measurement result is shown in Fig. 6. From Fig. 6, a 3.105Vpp modulation (volts peak-to-peak, upper waveform) produced a 346.2 mVpp output (lower waveform). Based on this result, the $V_\pi L$ value when driving one waveguide was determined to be 10.55 V cm, assuming quadrature point operation and a cosine squared model for the MZM transmission characteristic. Near-quadrature bias operation was

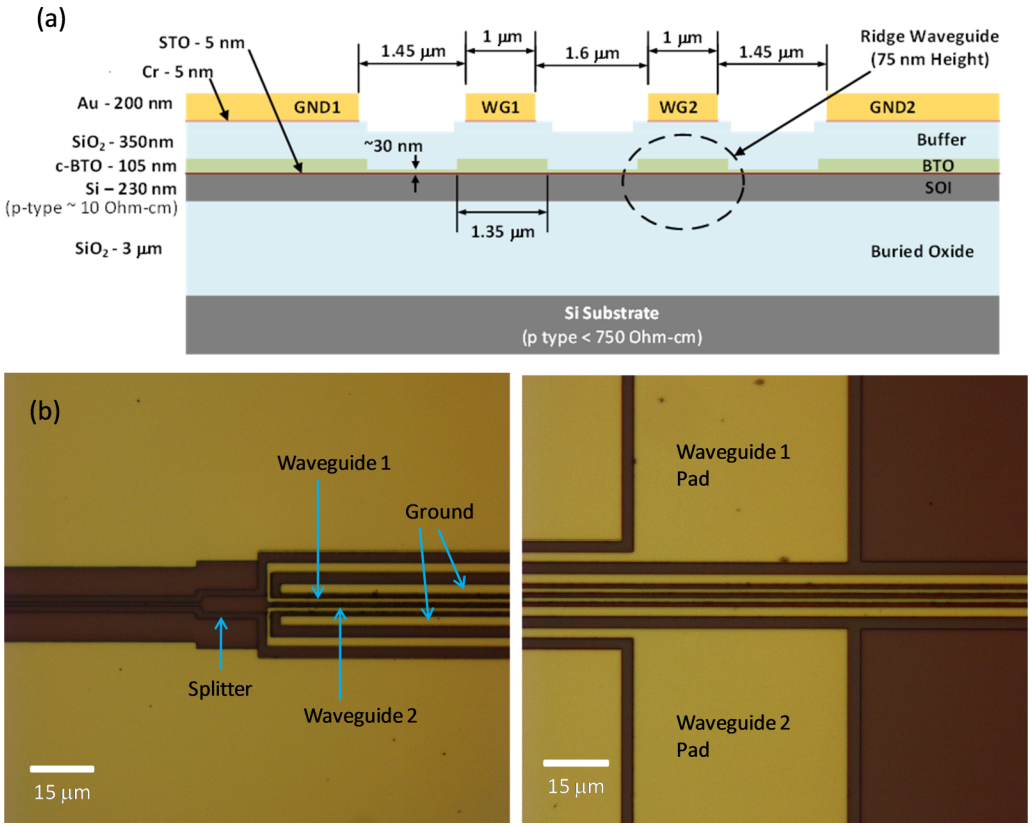

FIG. 5. (a) Cross-sectional geometry of the Z-cut BTO MZI modulator test device; (b) optical microscope images of the fabricated device: splitter and electrode feed section (left), and RF pads (right).

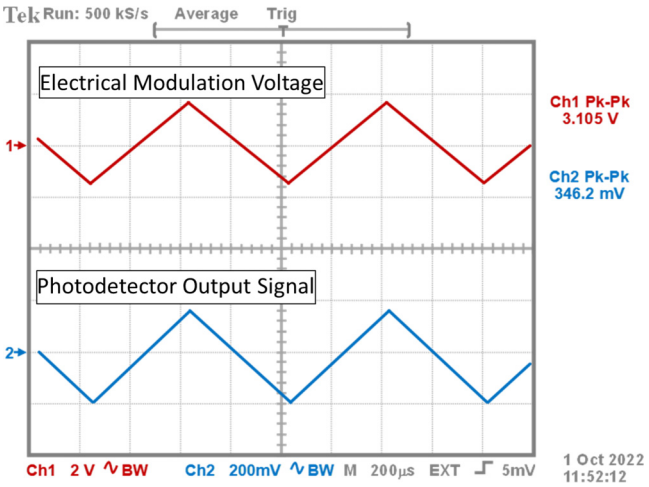

FIG. 6. Oscilloscope data when driving one waveguide electrode of a 1 mm length Z-cut BTO MZM modulator device.

confirmed through separate lock-in amplifier measurements of first and second order modulation products.

The simulated quasistatic E-field map for 1 V applied to the fabricated test MZM device is shown in Fig. 7. The portion of the TM (vertically) polarized optical mode in the BTO layer is shown in the inset image and was calculated using RSOFT BEAMPROP software. The relative dielectric constants for the materials were as follows: $\varepsilon_{BTO} = 56$ in the surface normal c-direction and 1200 in-plane, $\varepsilon_{SiO_2} = 4$, $\varepsilon_{Si} = 12$ with a conductivity $\sigma_{Si} = 10\,\Omega\,\text{cm}$. From this simulation data, the average vertically aligned E field within and around the peak of the BTO optical mode was 30 kV/m at 1 V applied.

For the BTO ridge-loaded waveguide design, the small signal change in optical waveguide mode index (Δn_{WG}) with change in the BTO material index (Δn_{BTO}) was simulated in RSOFT BEAMPROP software to be $\Delta n_{WG}/\Delta n_{BTO} = 0.32 = \delta$. The same modeling and simulation tool was used to calculate a transverse magnetic (TM) polarized optical waveguide index $n_{WG} = 2.344$. The r_{33} coefficient represented the change in BTO material index along the (vertical) c-direction with applied E-field along the c-direction. Using the measured $V_\pi L = 10.55$ V cm when modulating one waveguide of the MZM test device, the r_{33} electro-optic coefficient value for the BTO film was extracted via the Pockels model as follows:

$$\Delta n_{BTO}/V = r_{33}\left(\frac{E}{V}\right) n_{BTO}^3/2. \tag{4}$$

Rearranging terms and assuming 1 V applied produces Eq. (3), which is repeated here,

$$r_{33} = 2\Delta n_{BTO}/(En_{BTO}^3), \tag{5}$$

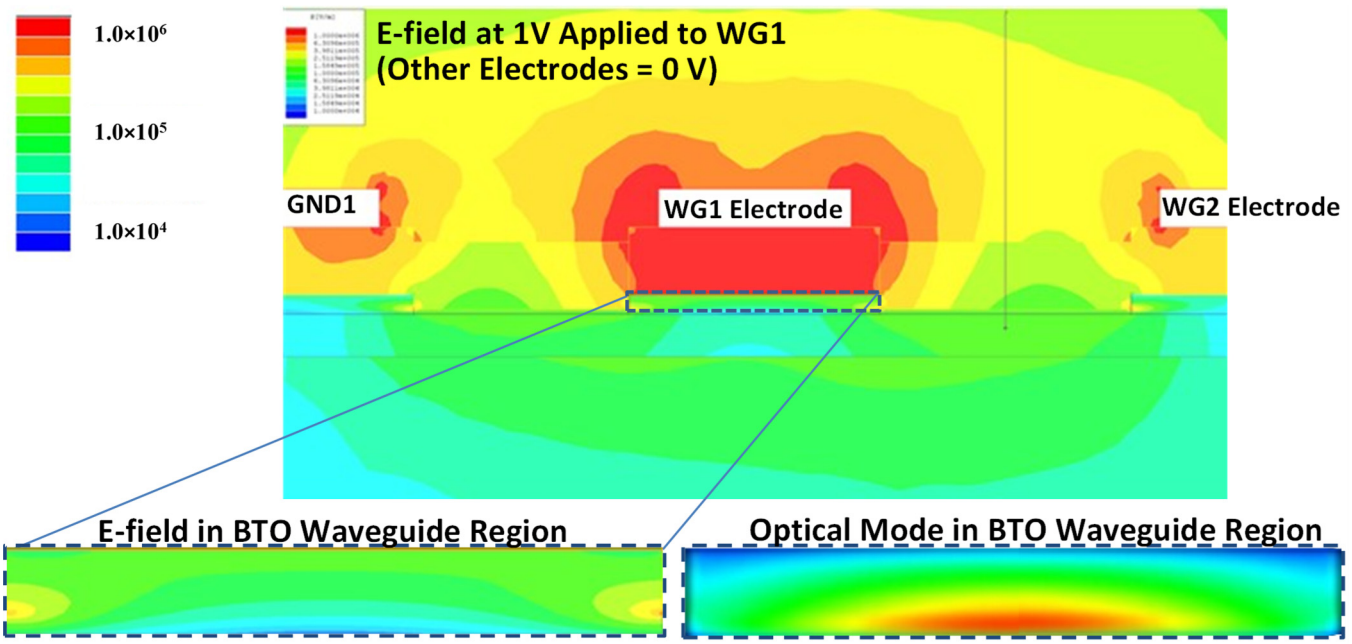

FIG. 7. Quasistatic E-field map for 1 V applied to the WG1 electrode. Due to strong dielectric anisotropy, the E-field direction in the BTO aligns primarily to the c axis of the film (i.e., vertical).

with

$$\Delta n_{BTO}/V = \Delta n_{WG}/(V\delta). \quad (6)$$

The change in waveguide index with voltage can be extracted from the measurement data by

$$\Delta n_{WG}/V = \lambda_0/(2V_\pi L). \quad (7)$$

Substituting terms, for 1 V applied

$$r_{33} = \frac{\lambda_0}{V_\pi L \delta (E/V) n_{BTO}^3}, \quad (8)$$

where E = c-aligned field in BTO per 1 V applied = 30 000 V/m/V, λ_0 = 1550 nm, n_{BTO} = 2.25 (for light polarized along the c-direction), δ = 0.32, measured $V_\pi L$ = 10.55 V cm, resulting in r_{33} = 134.4 pm/V.

VI. DISCUSSION

EO slab measurements were limited to 90 Hz due to limitations of the prism coupling test set-up. Piezo-coupled EO modes typically exhibit narrow spectral features that were not observed in the MZI device tests. The fact that the thin-film BTO MZM device response was relatively flat to 10 MHz bandwidth indicated that the extracted ***r*** value was, indeed, primarily due to the Pockels r_{33} coefficient for the BTO material. We have also observed that purely c-oriented films produced by sputter growth generally produce less strained BTO material, relative to a-oriented films, with the c-oriented material being closer to bulk crystal in material properties.[15] Bulk relaxed BTO has a typical reported r_{33} coefficient of between 90 to 110 pm/V. In slightly compressively strained MBE-grown a-cut films, an r_{33} value of ~300 pm/V has been claimed.[13] The measured enhanced value of 134.4 pm/V for the Z-cut material indicated that the BTO film may have benefited from residual strain. It is also important to note that the dielectric constant of the BTO will have a major impact on the extracted r coefficient. The bulk relative permittivity of 56 along the surface normal c-direction (ε_{33}) was assumed for the modeling and simulations, based on literature reports for high-quality thin BTO films.[23,24] However, the r_{33} value extracted from this work is considered to represent a minimum value. The actual surface normal-directed permittivity of the BTO film may be somewhat larger than 56, since films with thicknesses of 100 nm or greater may have a non-zero amount of very high permittivity a-oriented material. Based on these arguments, the r_{33} coefficient is expected to be at least 134.4 pm/V, and could be slightly higher, depending on the actual c-oriented permittivity of the material.

VII. CONCLUSIONS

Electro-optic (EO) grade BTO was grown in a Z-cut configuration on SOI photonic substrates via a high-speed sputter deposition process. Measured slab mode optical losses were on the order of 1–2 dB/cm for both TE and TM modes. EO measurements of a ridge waveguide MZI test device indicated an r_{33} value of at least 134 pm/V. Integrated EO devices are currently being prototyped to determine high frequency modulation performance.

ACKNOWLEDGMENTS

This work was done under support of U.S. Air Force Contract No. FA8649-20-C-0336 and the Air Force Office of Scientific Research under Grant No. FA9550-18-1-0053. The views expressed are those of the authors and do not reflect the official policy or position of the Department of Defense or the U.S. Government.

AUTHOR DECLARATIONS

Conflict of Interest

The authors have no conflicts to disclose.

Author Contributions

Agham B. Posadas: Conceptualization (equal); Data curation (equal); Formal analysis (equal); Methodology (equal); Writing – original draft (equal); Writing – review & editing (equal). **Vincent E. Stenger:** Conceptualization (equal); Data curation (equal); Formal analysis (equal); Funding acquisition (equal); Project administration (equal); Supervision (equal); Writing – original draft (equal); Writing – review & editing (equal). **John DeFouw:** Data curation (equal); Formal analysis (equal); Investigation (equal); Methodology (equal); Validation (equal). **Jamie H. Warner:** Formal analysis (equal); Investigation (equal); Resources (equal); Visualization (equal); Writing – review & editing (equal). **Alexander A. Demkov:** Conceptualization (equal); Formal analysis (equal); Funding acquisition (equal); Methodology (equal); Project administration (equal); Supervision (equal); Validation (equal); Writing – original draft (equal); Writing – review & editing (equal).

DATA AVAILABILITY

The data that support the findings of this study are available from the corresponding author upon reasonable request.

REFERENCES

[1]A. Rahim, A. Hermans, B. Wohlfeil, D. Petousi, B. Kuyken, D. Van Thourhout, and R. Baetsa, "Taking silicon photonics modulators to a higher performance level: State-of-the-art and a review of new technologies," Adv. Photonics **3**, 024003 (2021).
[2]H. Mekawey, M. Elsayed, Y. Ismail, and M. A. Swillam, "Optical interconnects finally seeing the light in silicon photonics: Past the hype," Nanomaterials **12**, 485 (2022).
[3]Y. Shi, Y. Zhang, Y. Wan, Y. Yu, Y. Zhang, X. Hu, X. Xiao, H. Xu, L. Zhang, and B. Pan, "Silicon photonics for high-capacity data communications," Photonics. Res. **10**, A106 (2022).
[4]A. A. Demkov and A. B. Posadas, "Si-integrated ferroelectrics for photonics and optical computing," MRS Bull. **47**, 485–493 (2022).
[5]G. Sinatkas, T. Christopoulos, O. Tsilipakos, and E. E. Kriezis, "Electro-optic modulation in integrated photonics," J. Appl. Phys. **130**, 010901 (2021).
[6]P. Rabiei, J. Ma, S. Khan, J. Chiles, and S. Fathpour, "Heterogeneous lithium niobate photonics on silicon substrates," Opt. Express **21**, 25573 (2013).
[7]C. Maleville and C. Mazuré, "Smart-cut® technology: From 300 mm ultrathin SOI production to advanced engineered substrates," Soldid-State Electron. **48**, 1055–1063 (2004).

[8]M. Li, J. Ling, Y. He, U. A. Yavid, S. Xue, and Q. Lin, "Lithium niobate photonic-crystal electro-optic modulator," Nat. Commun. **11**, 4123 (2020).
[9]M. Zhang, C. Wang, P. Kharel, D. Zhu, and M. Lončar, "Integrated lithium niobate electro-optic modulators: When performance meets scalability," Optica **8**, 652 (2021).
[10]C. Wang, M. Zhang, X. Chen, M. Bertrand, A. Shams-Ansari, S. Chandrasekhar, P. Winzer, and M. Lončar, "Integrated lithium niobate electro-optic modulators operating at CMOS-compatible voltages," Nature **562**, 101–104 (2018).
[11]M. He, M. Xu, Y. Ren, J. Jian, Z. Ruan, Y. Xu, S. Gao, S. Sun, X. Wen, L. Zhou, L. Liu, C. Guo, H. Chen, S. Yu, L. Liu, and X. Cai, "High-performance hybrid silicon and lithium niobate Mach–Zehnder modulators for 100 gbit s^{-1} and beyond," Nat. Photonics **13**, 359–364 (2019).
[12]W. Guo, A. B. Posadas, and A. A. Demkov, "Epitaxial integration of $BaTiO_3$ on Si for electro-optic applications," J. Vac. Sci. Technol. A **39**, 030804 (2021).
[13]S. Abel, T. Stöferle, C. Marchiori, C. Rossel, M. D. Rossell, R. Erni, D. Caimi, M. Sousa, A. Chelnokov, B. J. Offrein, and J. Fompeyrine, "A strong electro-optically active lead-free ferroelectric integrated on silicon," Nat. Commun. **4**, 1671 (2013).
[14]F. Eltes, C. Mai, D. Caimi, M. Kroh, Y. Popoff, G. Winzer, D. Petousi, S. Lischke, J. E. Ortmann, L. Czornomaz, L. Zimmermann, J. Fompeyrine, and S. Abel, "A $BaTiO_3$-based electro-optic Pockels modulator monolithically integrated on an advanced silicon photonics platform," J. Lightwave Technol. **37**, 1456–1462 (2019).
[15]A. B. Posadas, H. Park, M. Reynaud, W. Cao, J. D. Reynolds, W. Guo, V. Jeyaselvan, I. Beskin, G. Z. Mashanovich, J. H. Warner, and A. A. Demkov, "Thick $BaTiO_3$ epitaxial films integrated on Si by RF sputtering for electro-optic modulators in Si photonics," ACS Appl. Mater. Interfaces **13**, 51230–51244 (2021).
[16]C. Xiong, W. H. P. Pernice, J. H. Ngai, J. W. Reiner, D. Kumah, F. J. Walker, C. H. Ahn, and H. X. Tang, "Active silicon integrated nanophotonics: Ferroelectric $BaTiO_3$ devices," Nano Lett. **14**, 1419–1425 (2014).
[17]S. Abel, F. Eltes, J. E. Ortmann, A. Messner, P. Castera, T. Wagner, D. Urbonas, A. Rosa, A. M. Gutierrez, D. Tulli, P. Ma, B. Baeuerle, A. Josten, W. Heni, D. Caimi, L. Czornomaz, A. A. Demkov, J. Leuthold, P. Sanchis, and J. Fompeyrine, "Large Pockels effect in micro- and nanostructured barium titanate integrated on silicon," Nat. Mater. **18**, 42–47 (2019).
[18]F. Eltes, D. Caimi, F. Fallegger, M. Sousa, E. O'Connor, M. D. Rossell, B. Offrein, J. Fompeyrine, and S. Abel, "Low-loss $BaTiO_3$–Si waveguides for nonlinear integrated photonics," ACS Photonics **3**, 1698–1703 (2016).
[19]A. A. Demkov, C. Bajaj, J. G. Ekerdt, C. J. Palmström, and S. J. Ben Yoo, "Materials for emergent silicon-integrated optical computing," J. Appl. Phys. **130**, 070907 (2021).
[20]P. Stark, F. Horst, R. Dangel, J. Weiss, and B. J. Offrein, "Opportunities for integrated photonic neural networks," Nanophotonics **9**, 4221–4232 (2020).
[21]D. Moor, J. Winiger, P. Ma, A. Messner, B. I. Bitachon, S. Abel, F. Eltes, J. Fompeyrine, and J. Leuthold, ">150 GHz hybrid-plasmonic $BaTiO_3$-on-SOI modulator for CMOS foundry integration," in *Frontiers in Optics + Laser Science 2021*, edited by C. Mazzali, T.(T.-C.) Poon, R. Averitt, and R. Kaindl (Optica Publishing Group, 2021), paper FTh4D.2, Technical Digest Series.
[22]H. Li, X. Hu, Y. Wei, Z. Yu, X. Zhang, R. Droopad, A. A. Demkov, J. Edwards, K. Moore, W. Ooms, J. Kulik, and P. Fejes, "Two-dimensional growth of high-quality strontium titanate thin films on Si," J. Appl. Phys. **93**, 4521 (2003).
[23]M. Zgonik, P. Bernasconi, M. Duelli, R. Schlesser, P. Günter, M. H. Garrett, D. Rytz, Y. Zhu, and X. Wu, "Dielectric, elastic, piezoelectric, electro-optic, and elasto-optic tensors of $BaTiO_3$ crystals," Phys. Rev. B **50**, 5941–5949 (1994).
[24]A. Rosa, D. Tulli, P. Castera, A. M. Gutierrez, A. Griol, M. Baquero, B. Vilquin, F. Eltes, S. Abel, J. Fompeyrine, and P. Sanchis, "Barium titanate ($BaTiO_3$) RF characterization for application in electro-optic modulators," Opt. Mater. Express **7**, 4328 (2017).